Heritage Science

RESEARCH

Open Access

Secrets on the rock: analysis and discussion of the Dunde Bulaq rock art site

Fu Yihao[1†], Chai Yue[2†], Wang Jun[1], Liu Cheng[2*], Zhang Xiaoyu[2], Li Lu[2], Zhuoya Baheti[3] and Peng Jinye[1*]

Abstract

The Altay Prefecture in Xinjiang Uyghur Autonomous Region, China, boasts an abundance source of rock art, with the Dunde Bulaq rock art complex holding paramount significance in the study of local culture. This work employs hyperspectral techniques for data collection and analysis of the Dunde Bulaq I rock art site. Signal decomposition, pigment classification/clustering, and spectral curve analysis were employed to delve deeply into the information of the rock art hyperspectral data. Furthermore, cross-validation was utilized to reveal hidden information within rock art. To comprehend these hidden information, a more profound historical tracing was conducted, employing methods such as literature retrieval and image analysis, uncovering the internal relationship between the site I and the Chemurchek culture. This provides fresh material for studying the Bronze Age cultures within the Altai region.

Keywords Rock art, Dunde Bulaq, Chemurchek culture, Hyperspectral image analysis

Introduction

Rock art is one of the most important medium for ancient population to express themselves and communicate with others during the prehistory. It serves as significant material evidence for understanding the living environment, livelihood methods, spiritual beliefs, and other aspects of ancient peoples in different regions [1]. Additionally, it is also one of the most essential materials for interpreting and reconstructing the development process of human culture. Rock art research had begun in 19*th* century. Then with the official confirmation of the authenticity of Franco-Cantabrian cave art in the early 20th century, rock art research has gradually gained attention from various fields [2–4].

As one of the centers of ancient civilization and a crossroad of East-West cultural exchange, the Altai region possesses abundant rock art resources and has been a core area for rock art research. Geographically, the Altai region mainly refers to the Altai Mountains and adjacent areas, and Xinjiang's Altay Prefecture in China being an important component. It is located in the heartland of the Eurasian continent, bordering Kazakhstan, Russia, and Mongolia. The stone artifacts from the Tongtian Dong site in Jeminay County representing the Levallois-Mousterian culture, exhibit distinct characteristics of the Middle Paleolithic culture of the western side of the Old World [5]. The Chemurchek culture, characterized by olive-shaped round-bottomed jars and standing stone acompanied with burials found in burial sites, demonstrates the Altay Prefecture had extensive connections with the adjacent areas in Bronze Age and Iron Age [6]. These archaeological findings indicate that the development of prehistoric cultures in the Xinjiang Altai region was influenced by both Eastern and Western as well as Northern and Southern cultural factors. As the most abundant material cultural remains in the region, rock art

[†]Fu Yihao and Chai Yue are contributed equally to this work.

*Correspondence:
Liu Cheng
liucheng@nwu.edu.cn
Peng Jinye
pjyxida@nwu.edu.cn
[1] School of Information Science & Technology, Northwest University, NO.1, Xuefu Street, Xi'an 710127, Shaanxi, China
[2] School of Cultural Heritage, Northwest University, NO.1, Xuefu Street, Xi'an 710127, Shaanxi, China
[3] Altai Regional Museum, NO.193, Tuanjie Street, Altay Region, Xinjiang Uygur Autonomous Region, China

also reveals extensive connections with Central Asia and Siberia [7].

In the 1960s, Wang et al. [8] conducted a systematic survey of rock art sites in the Xinjiang's Altay Prefecture, discovering numerous painted rock art sites at various locations, such as Aketasi in Altay City, Tanblatas in Fuyun County, and Dugart in Kaba County. Zhang et al. [9] conducted research on the content, chronology, and ethnicity of cave rock art in Fuyun County and Kaba County, linking them to prehistoric shamanistic activities of the Mongolian era. Between 1994 and 2001, the joint Mongolian-Russian-American team [10] found rock art in Mongolia's Altai Mountains spanning from the Stone Age to the early Iron Age, mostly concentrated in the Bronze to early Iron Ages. Vanwezer et al. [11] documented three new rock art sites in Mongolia's Gobi Altai Mountains, comparing them with early Mongolian rock art and associating them with Neolithic anthropomorphic imagery. O'Sullivan [12] used space analytical tool of GIS in the Altai region and found that most rock art sites were strategically located along major transportation routes, suggesting their role in communication and recording socio-political aspects. Díaz-Andreu et al. [13] analyzed three rock art sites in the lower Chuja River area based on acoustics method, suggesting a correlation with sound, speech, or musical rituals. In this region, the count and richness of rock art stand in stark contrast to the laborious and time-consuming nature of traditional analysis methods [14, 15]. It has been a tendency to study rock art from the multidisciplinary perspective. Among various analytical methods, non-invasive and non-contact spectroscopic analysis techniques are increasingly garnering attention.

As one of the emerging technologies in image analysis, hyperspectral technology has been widely applied in the cultural heritage field for disease segmentation and classification [16, 17], cultural heritage restoration [18, 19], and implicit information extraction [20–23]. This technology can capture information across various spectral bands, ranging from ultraviolet to infrared wavelengths, within the target area, while maintaining a "non-contact, non-destructive" characteristic [24]. Moreover, this technique is often combined with other analytical methods and has been proven to be an effective tool for identification tasks, material analysis, and artwork restoration [25–27]. In the field of cultural heritage, Wang et al. [17] proposed an automated identification and recognition method for categorizing corrosion types of bronze artifacts based on the spectral differences between different types of corrosion and bronze. Peng et al. [22] analyzed and explored the implicit information in painted cultural relics by fusing principal component images with hyperspectral images (HSIs). Zhang et al. [23] conducted an analysis of Tang Dynasty mural paintings using hyperspectral technology and applied non-negative matrix underapproximation to extract the underlying sketches of murals. In recent years, hyperspectral technology has begun to be applied in the analysis research of rock art [25, 28]. Skoog et al. [29] were unsatisfied with the accuracy of the generic unsupervised classification algorithm (*K*-means) to detect rock art in Walga Rock, Australia. However, they encourage other classification algorithms to be trialed [29, 30]. Bernard et al. [20] compared the use of hyperspectral technology with RGB image technology in rock art scenes, and found that compared with RGB image technology, hyperspectral technology can not only reveal disappeared paintings but also analyze the overlapping relationships of images. Claudia et al. [21] used hyperspectral technology to excavate additional hidden patterns at the Otello rock shelter (Saint-Rémy-de-Provence, France). In addition, through pigment classification and analysis of hyperspectral data, this team discovered personalized patterns in overlapping paintings. According to a limited number of published studies, hyperspectral technology has demonstrated its ability to extract and unearth additional hidden information in rock art [25, 28]. It can unveil underlying pigment layers, revealing the original state of rock art and providing visual evidence for exploring its formation period.

In this work, our research team utilized hyperspectral imaging technology to collect data from the Dunde Bulaq rock art site whicn are composed of five shelters. Through techniques such as signal decomposition, pigment classification and clustering, and spectral band/curve analysis, we conducted a comprehensive discussion and analysis of the rock art in this area. Firstly, we introduced a novel approach by employing cross-validation to interpret the pictorial information and uncover hidden painting details within the rock art. By combining pigment classification and clustering methods, we have revealed hidden paintings that have never been discovered before. Furthermore, our investigation of these hidden painting details provided new evidence for dating certain images depicted in the rock art of this region. Lastly, this study succeeded in unveiling previously hidden images within the Dunde Bulaq I rock art site, which is the most important component of the Dunde Bulaq complex. This discovery provides valuable historical evidence that can be utilized by disciplines such as archaeology and anthropology to gain a deeper understanding of the region's cultural heritage.

The subsequent sections are organized as follows. Section "Location description, Data collection & Methodology" provides an overview of data collection and methodology. Section "Results from the Dunde

Fig. 1 Aerial view of the surrounding environment of Dunde Bulaq I rock art site

Bulaq rock art site" presents the results. Section "Discussion" engages in discussion. And finally, a conclusion is presented.

Location description, data collection & methodology

Description of the site

The Dunde Bulaq rock art complex is located approximately 4 kms northeast of Handegat Mongolian Autonomous Township in Altay Prefecture, Xinjiang Uyghur Autonomous Region (Fig. 1). The location map of Dunde Bulaq rock art complex is shown in Fig. 2. The opening of Dunde Bulaq I rock art site faces almost south. The overall dimensions of Dunde Bulaq I rock art site are 3.23 ms in width and 1.18 ms in height. Dunde Bulaq II rock art site faces southwest, and it has a width of 6.1 ms, height of 2.3 ms, and depth of 2.4 ms.

Device information

The sites were captured using SPECIM IQ cameras, as shown in Fig. 3a, b. The device is an HSI system operating in VNIR that captures spectral information based on

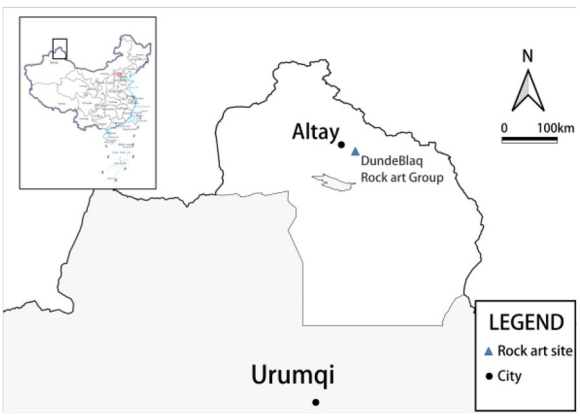

Fig. 2 Site location map of Dunde Bulaq rock art complex

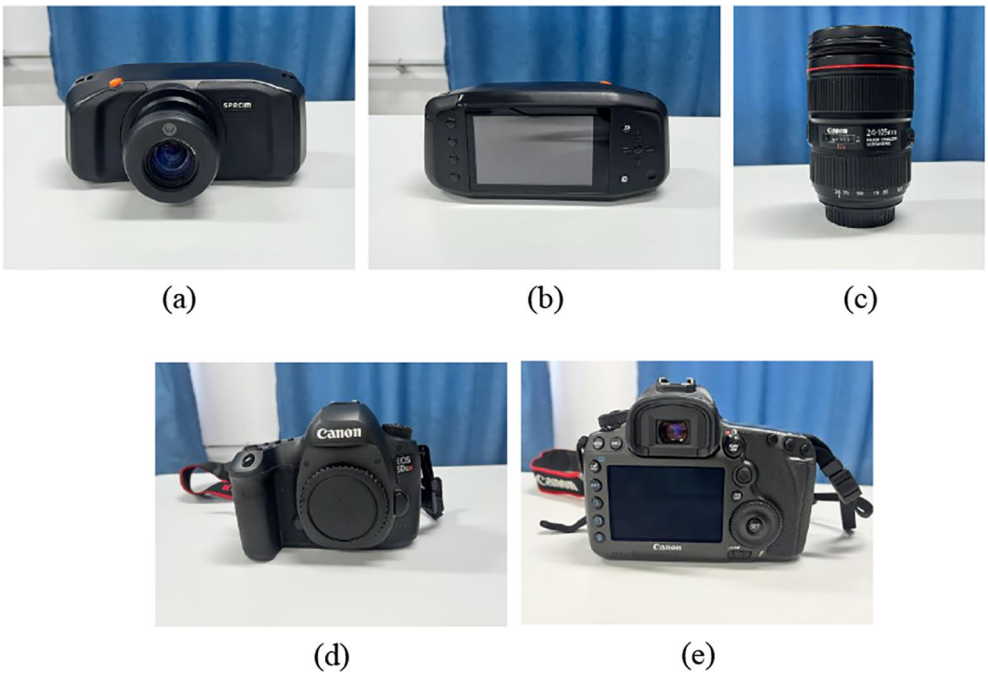

Fig. 3 Data collection equipment. **a** SPECIM IQ camera front; **b** SPECIM IQ camera back; **c** EF 24–105 mmf/4 L IS USM; **d** Canon 5DS R camera front; **e** Canon 5DS R camera back

the principle of internal line scanning. It covers the entire wavelength range of $400nm \sim 1000nm$ with a spectral resolution of $7nm$. The parameters of the camera are shown in Table 1 [20, 31]. The camera is also equipped with a 1.2-megapixel RGB image sensor that has slightly higher resolution than the HSI image. Moreover, it is capable of capturing images almost simultaneously with the spectral image under the same conditions and from the same angle ($2.5cm$ higher than the HSI lens).

Due to the susceptibility of spectral information to lighting conditions, sunlight is used as the light source in the scenes presented. This sunlight is scattered by the surrounding environment on completely clear days, resulting in completely uniform illumination for rock paintings. During the acquisition process, although changes in the intensity of light may occur due to time changes, changes in illumination during the scanning period (< 3 minutes) can be ignored. However, adverse factors such as extreme values and noise may have a negative impact on the image analysis of rock paintings. Therefore, hyperspectral data is limited to the range of $400nm \sim 940nm$, which includes 184 spectral bands (rather than the full 204 bands).

For panoramic image acquisition, the Canon 5DS R camera was utilized alongside the EF $24 - 105mm$ f/4 L IS USM lens to capture on-site visuals (Fig. 3c–e). The collected camera photos were subsequently stitched together using the PTGui panorama creation tool to produce high-quality panoramic images.

Hyperspectral image analysis methods

Standard ENVI HSI software (version 5.3) was used in this work to analyze hyperspectral data collected at different locations using various standard tools provided by the software. The results were compared with simultaneously recorded RGB images and high-resolution images of the same scene captured by different cameras, and analyzed using ENVI.

Two machine learning algorithms were used to identify component information, and an unsupervised clustering algorithm was applied for signal extraction in hyperspectral data component analysis:

- Independent component analysis (ICA), a commonly used algorithm for signal processing and data analysis [32], aims to recover mutually independent components from mixed signals.

- Spectral angle mapping (SAM), a supervised classification algorithm based on the principle of spectral similarity [28], can rapidly and accurately perform land cover classification and target detection.
- *K*-means clustering (*K*-Means), a common unsupervised clustering algorithm, aims to automatically identify and cluster component features from data.

The basic principle of ICA is to assume that the mixed signals can be expressed as a linear combination of independent components, where each component is statistically independent from each other. By applying inverse transformation to the observed mixed signals, the independent components can be obtained and thus the mixed signals can be separated. ICA is widely used in scenarios such as speech signal separation, financial data analysis, and image processing. Due to its strong signal separation capability, ICA has been applied in rock art analysis [20, 21] in recent years to analyze the composition information and superimposed relationships in images.

SAM is a spectral classification algorithm based on the comparison between a pixel and a reference spectrum in an *N*-dimensional space. This algorithm determines the similarity between two spectra by calculating the angle between them, and any pixel with an angle greater than a specified maximum angle threshold will not be classified into that class [21]. A larger threshold allows for a higher tolerance of spectral similarity but reduces classification accuracy, while a smaller threshold improves classification accuracy but decreases the tolerance for spectral similarity [20, 21]. It can be expressed as:

$$SAM(x,y) = cos^{-1}\left(\frac{\langle x,y\rangle}{\|x\|\|y\|}\right) \quad (1)$$

where x represents unknown pixels, y represents known pixels, $< x,y >= x \cdot y$ denotes the dot product between x and y, $\|\cdot\|$ signifies the L_2-norm operation.

K-Means involves computing initial class means that are uniformly distributed in data space, and then iteratively assigning the pixels to the nearest class using the shortest distance technique. In each iteration, the class means are recomputed and used to classify the pixels again [33, 34]. The pseudo-code of the algorithm is shown in the Algorithm 1.

Diverging from other researches, our research opts not to rely on the conventional methods of Minimum Noise Fraction (MNF) and Principal Component Analysis [28, 30] as the primary analytical tools, instead employing ICA. This choice stems from MNF predominantly serving for dimensionality reduction and noise handling in HSIs [35] (utilized in Section "Simple invisible scene"), while ICA excels in signal separation [36]. Hence, the use of ICA is advantageous for the overlay and analysis of rock art HSIs. For information recognition, our research combines unsupervised and supervised methods to perform cross-validation. All these methodologies can be replicated and found within the ENVI HSI software (Fig. 3).

Table 1 Features of Specim IQ hyperspectral imaging system and its RGB camera [31]

Hyperspectral imager	**SPECIM IQ**
Sensor type	CMOS
Spectral range	400 – 1000*nm*
Spectral resolution	7 *nm*
Spectral bands	204
Image size	512 × 512 px
Focal length	21 *mm*
Field of view (fixed lens)	31°× 31°
Imaged wall @1 m	55 × 55*cm*
Spatial resolution @1 m	1.07 *mm*
Focus range	15*cm* – ∞
Weight	1.3 *kg*
Context RGB image	
Image size	1280 × 960*px*
Imaged wall@1 m	110 × 82*cm*
Spatial resolution @1 m	0.85 *mm*

Algorithm 1 *K*-Means algorithm

1: Randomly initialize K cluster centroids $u_1, u_2, \ldots, u_k$
2: **repeat**
3: **for** $i = 1$ to m **do**
4: c_i:= index (from 1 to K) of cluster centroid closest to x_i
5: **end for**
6: **for** $k = 1$ to K **do**
7: u_k:= average (mean) of points assigned to cluster k
8: **end for**
9: **until** convergence

Results from the Dunde Bulaq rock art site

Here, we first present the panoramic stitching image of the Dunde Bulaq I (Fig. 4), followed by several representative painting scenes that demonstrate four types of

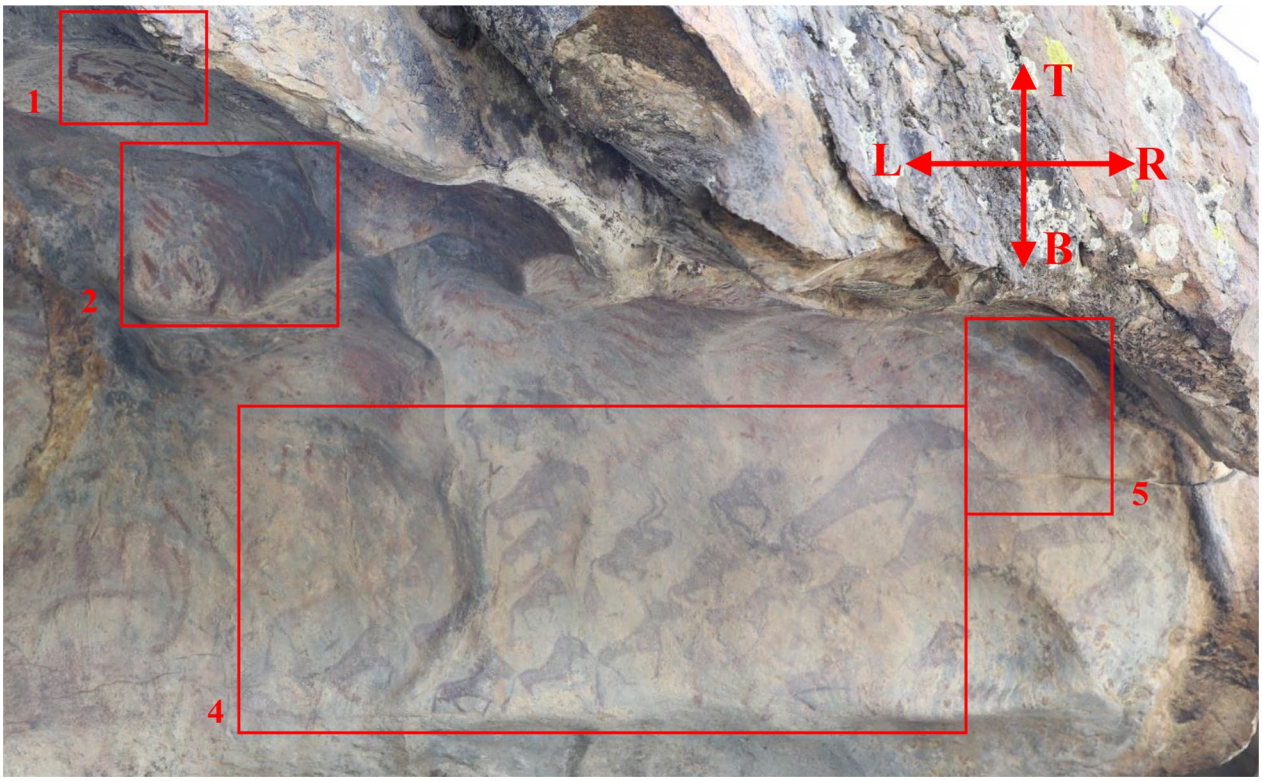

Fig. 4 Panoramic view of the front of the rock art at Dunde Bulaq I

painting scenarios, ranging from simple visible scenes to complex invisible scenes. In this comparison, the richer image information provided by HSIs relative to RGB images is highlighted.

ICA transformation is employed as the primary analytical method, and most of the information from the 184 spectral bands used is concentrated in 6 to 15 independent components, depending on the complexity of the rock material and the diversity of the paintings. Different images are usually decomposed into 2 to 4 independent components, mainly describing various pigments in the rock art. Other independent components contain different types of noise, sometimes mixed with trace pigment information. *K*-Means clustering and SAM classification are employed as main methods for extracting component information.

Before presenting the results, it's essential to establish certain definitions. The distinction between "simple" and "complex" scenes lies in the overlap of pigments in the painting, irrespective of the content depicted. The difference between "visible" and "invisible" hinges on whether the original painting is directly observable. "Invisible" denotes that the painting is nearly or completely invisible, and this information is also known as hidden information [22, 37, 38]. Additionally, the referential nouns used in this section to describe specific areas, such as "Horse" or "Human," are named because their shapes resemble certain common objects. This naming convention aims to facilitate differentiation and discussion rather than define the informational content within those specific areas.

Simple visible scenes

In Fig. 5, a simple visible scene is presented. In this panel, there might be one or two types of pigments, located within Region 1 in Fig. 6. The majority of information in the HSI is concentrated in the first 14 independent components obtained through ICA transformation. In Fig. 5, the information depicted primarily exists within the first two independent components (Fig. 5a, b), with only a small amount of contour information present in the third independent component. It is apparent that the use of ICA transformation on hyperspectral data yields image information that can distinctly separate pigment details on the rocks, as opposed to the image information contained within the RGB image itself. Comparing Fig. 5a, b, it is clearly that Fig. 5a mainly contains "Outline" information, while Fig. 5b focuses on "Blush" and partially includes information related to the "forehead" of the

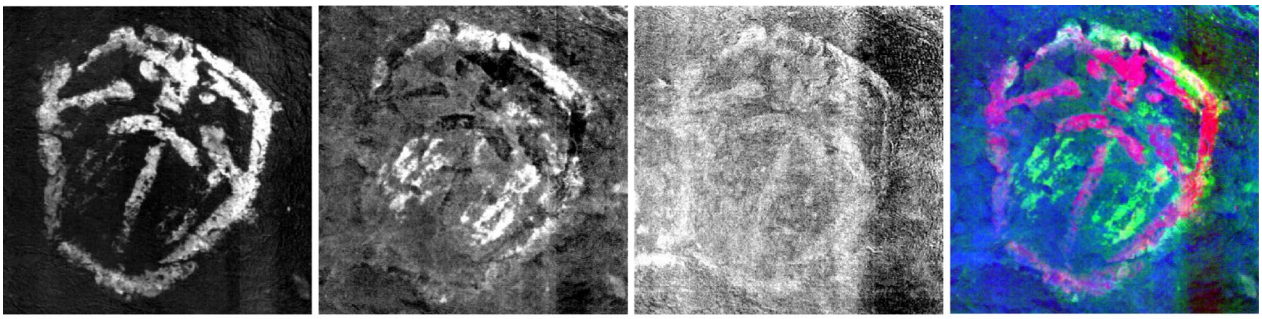

Fig. 5 The first three components of the ICA transformation are shown. **a** Component #1; **b** Component #2; **c** Component #3; **d** A false-color image composed of the first three components

"facial" information overlapping with Fig. 5a. Figure 5d also supports this overlap. It suggests that the overall depiction of the "facial" information may be the result of two production process.

The results obtained from SAM classification using ICA transformation for the "Outline" and "Blush" regions are shown in Fig. 6. The maximum angle threshold parameter of SAM is set to be 0.5. The curve analysis of ICA components reveals that, as shown in Fig. 7a, the "Outline" and "Blush" regions are primarily separated into the component #1 and #2 of ICA transformation, further confirming that these two regions are not part of the same information. Additionally, our team conducted an average spectrum analysis on the original 184 spectral bands data for the "Outline" and "Blush" regions. The results, depicted in Fig. 7b, show a significant difference between the average spectral curves for these two regions. Through a wavelength-by-wavelength analysis of the 184 bands for the "facial" information, as shown in Fig. 6, it is observed that before 410 nm, the right eye information of the "facial" information appears blurry. Between 580 nm and 600 nm, regions 1, 2, and 3 gradually disappear. After 660nm, the information from regions 1 and 3 is essentially vanish. Beyond 730nm, the image contains only "Outline" information. Compared with Fig. 4a, the information presented after 730 nm is also characterized by darker colors in visible light. Moreover, there are evident differences in pigment color between the "Outline" and regions 1, 2, and 3 in Fig. 8. This observation indirectly supports the hypothesis that there might be variations in the formation time of these two areas.

Finally, the extracted components are restored to the original image using a "grayscale conversion & overlay " technique (Fig. 9c), aiming to enhance the visual content on the surface of the rock and thereby better present the panel.

Complex visible scene

Figure 10 is considered a complex visible scene, located within Region 2 in Fig. 4. Due to the overall unevenness of the rock surface, the painting content cannot be discerned in Fig. 10f, but traces resembling manual smudges can be observed throughout the image. Although the image on the right side of Fig. 10f contains a similar deep red pigment, it is difficult to discern what it represents. However, by applying an ICA transformation to HSI, the deep red image on the right side of Fig. 10f is explained and interpreted.

In ICA transformation, all the information is concentrated in the first 12 components. The components associated with the "Smear" are primarily found in components #3 and #4 (Fig. 10b, c), while component #2 (Fig. 10a) only contains faint contour information. In Fig. 10c, the original deep red pigment information is separated, forming an overall image resembling a "deer". Strangely, at this site, the majority of animals face from left to right, as seen in Region 4 in Fig. 4, whereas the "deer" faces from bottom to top. Therefore, by rotating this area clockwise by 90°, we hypothesize that the "Smear" may represent the sky or clouds.

In the comparison between Fig. 10b, c, two obvious lines are also separated out on the left side of Fig. 10c. In Fig. 10f, these two thick lines were previously believed to be associated with the "Smear". Therefore, for the simple annotation of the components in the ICA transformation (a total of 10 classes), we deliberately divided the "Deer" and "Smear" into 2 classes. In the SAM, the maximum angle threshold parameter is set to 0.65. The resulting classification retained only the rock art information while removing irrelevant information such as the background and noise, as shown in Fig. 10h. In Fig. 10h, the yellow region is classified as belonging to the "Deer" and is relatively independent from the "Smear". Figure 11 shows the average curves of the SAM classified regions

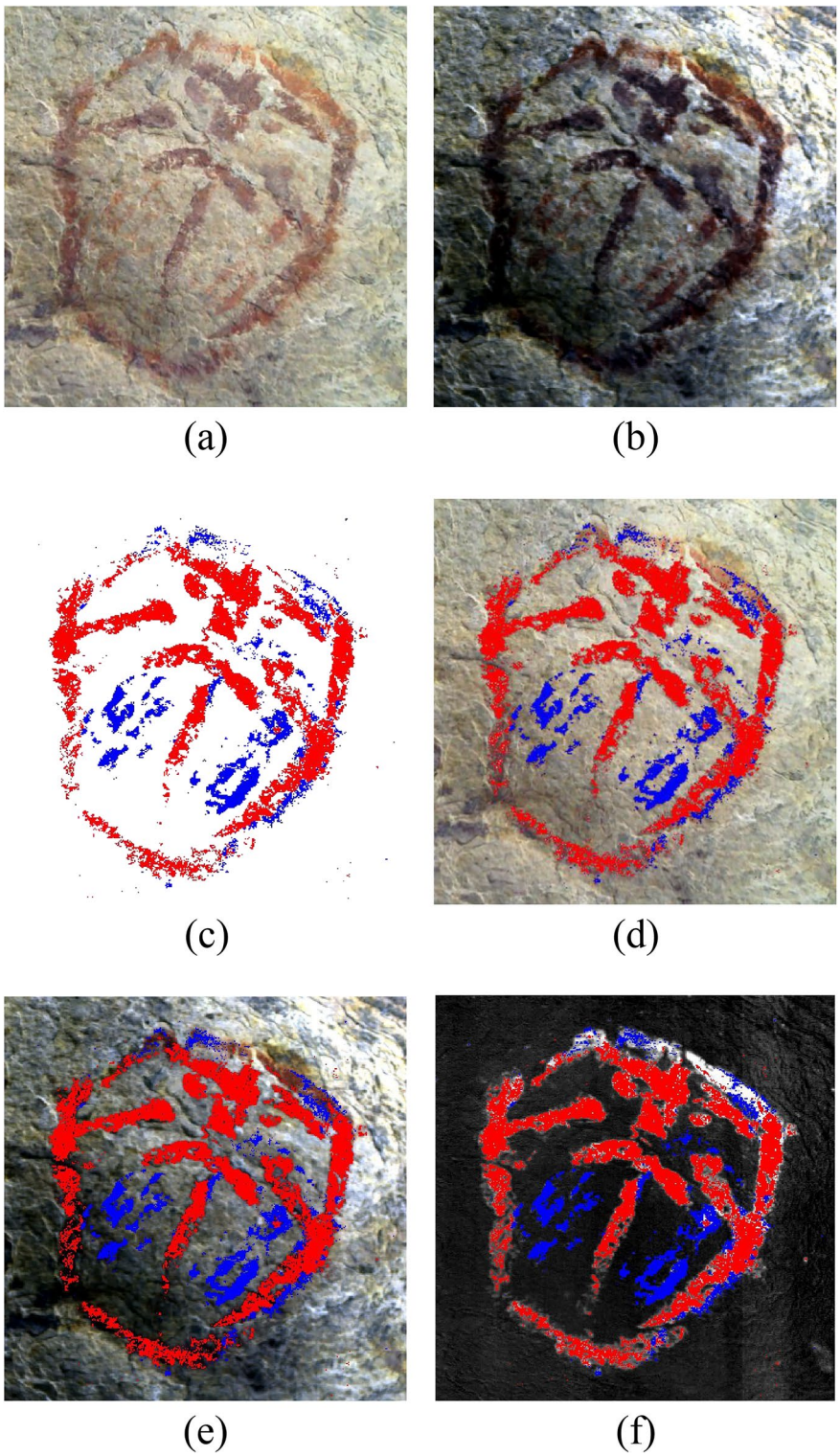

Fig. 6 The results of classifying ICA transformation by SAM are shown. **a** RGB images; **b** False color images of HSI (R:598.60 nm, G:548.55 nm, B:449.35 nm); **c** SAM classification results; (**d**) (**c**) is mapped to (**a**); (**e**) (**c**) is mapped to (**e**); (**f**) Map (**c**) to ICA component #1. To differentiate, the red area is named as "Outline," and the blue area as "Blush"

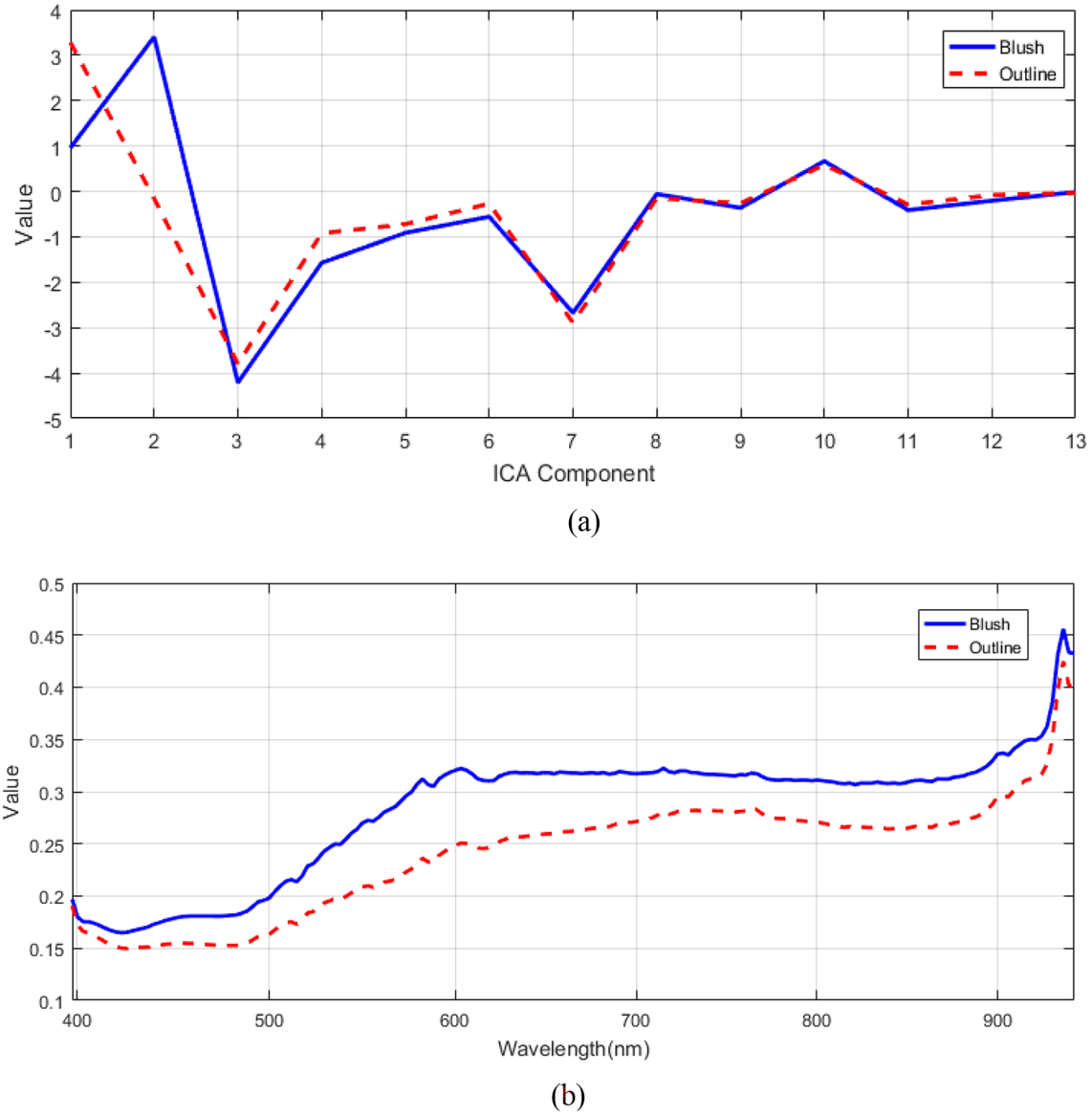

Fig. 7 The results of the information statistics on the "Blush" and "Outline" areas are shown. (**a**) Statistical curves of ICA components; (**b**) The mean spectral curve of the HSI

on the ICA components and hyperspectral image. From Fig. 11a, it can be observed that the "Deer" and "Smear" information differ the most between the components #2 and #4. In Fig. 11b, the spectral information shows more distinct differences before 580*nm*, while the differences become relatively constant after 580*nm*. Therefore, it can be inferred that this painting was created using different pigments.

Finally, in Fig. 10i, the components are reconstructed back into the original image using a "grayscale conversion & overlay" method, which emphasizes the image of "Deer".

Simple invisible scene

An an example of a simple hidden information scene, the result of the Dunde Bulaq II is presented in Fig. 12. From Fig. 12e, it can be observed that the overall information about the rock surface is virtually non-existent, with only the "Human" remaining identifiable. Additionally, there are traces of chalk on the rock surface and significant layer peeling. After performing ICA transformation on its 184 spectral bands, the main information of this rock art site is divided into 9 components. Among them, the hidden information ("Sheep") is excavated clearly. The overall information of the rock art ("Human" and

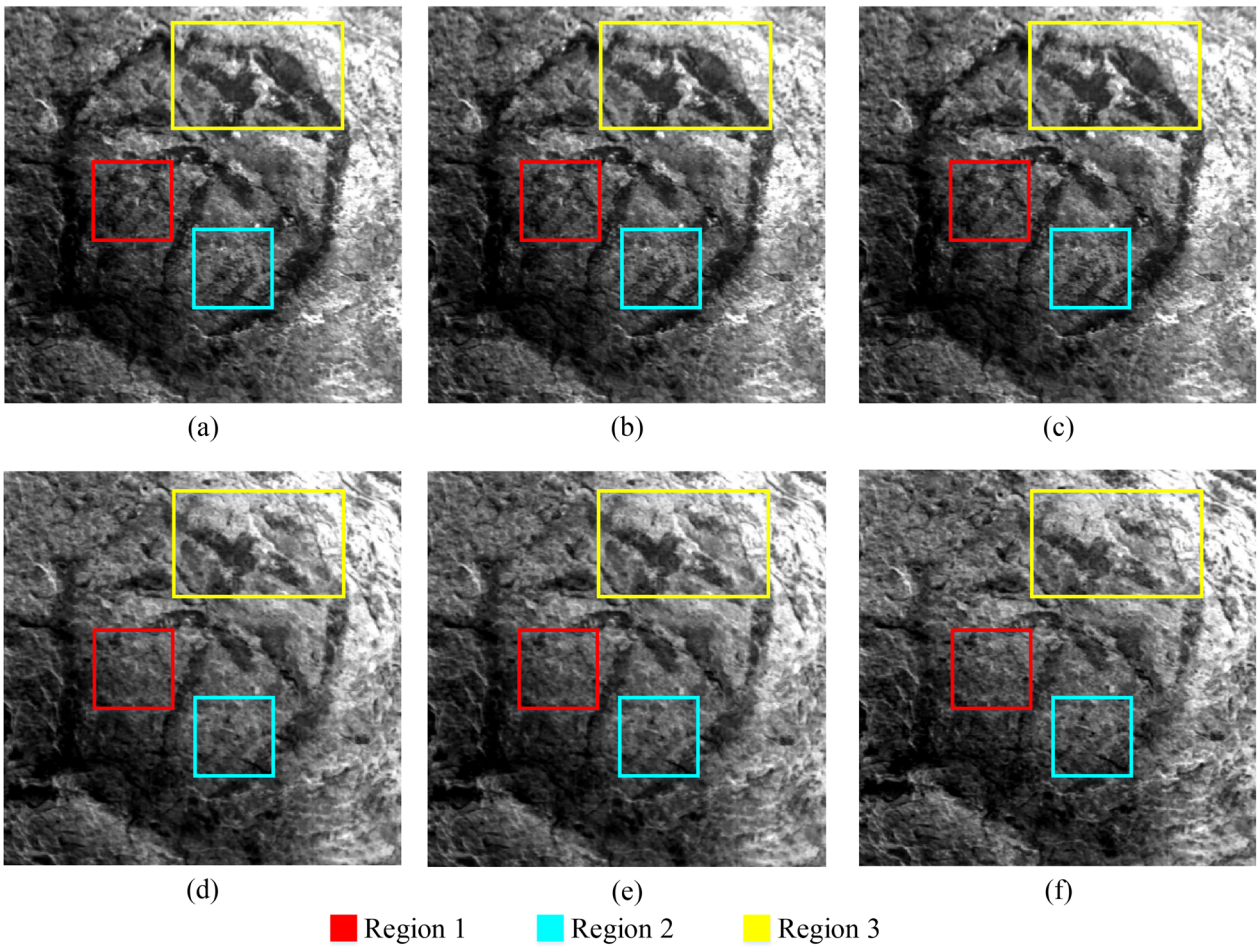

Fig. 8 In each band, the presentation of "facial" information. (**a**) 414 nm; (**b**) 550 nm; (**c**) 580 nm; (**d**) 660 nm; (**e**) 730 nm; (**f**) 801 nm

"Sheep") only exists in the components #2, #5, #7 of the ICA (Fig. 12b–d), while the traces of chalk only exist in the component #1 (Fig. 12a).

In order to determine whether the "Sheep" and "Human" were created using the same pigments, SAM classification is performed on the ICA components. The maximum angle threshold parameter for SAM classification is set to 0.3, and the classification result is shown in Fig. 13b. Due to the presence of a significant amount of noise, the results were subjected to denoising processing, resulting in Fig. 13c. In Fig. 13c, pixel mixing is observed in the classified areas of both the "Sheep" and "Human". The average spectral curves of these regions (Fig. 13e) show a consistent offset of approximately 0.069—0.075 (mean offset: 0.072) between the "Human" and "Sheep". Subtracting this 0.072 offset results in nearly complete overlap of their spectral curves. Therefore, it can be inferred that the "Sheep" and "Human" were created using the same pigments. The differences between them could be due to surface weathering and peeling of the "Sheep", causing spectral shifts.

Figure 12e, f reveal that, despite weathering and anthropogenic damage, as long as the pigment information remains intact (without destructive events like rock detachment or lichen corrosion), it is possible to explore and extract the pigment information to further unveil the historical significance encapsulated in the rock paintings.

Complex invisible scene

In this subsection, several representative case are presented. The first scene is the Region 4 in Fig. 4. Due to the inability to acquire HSI for the entire region in a single capture, a "region-by-region acquisition & stitching" approach was employed to collect it (Fig. 14). By using ICA transformation, the HSI not only separate the animal shapes that are almost unrecognizable to the naked eye ("Horse") completely, but also isolates a distinct shape (seemingly that of a "wild boar") at the

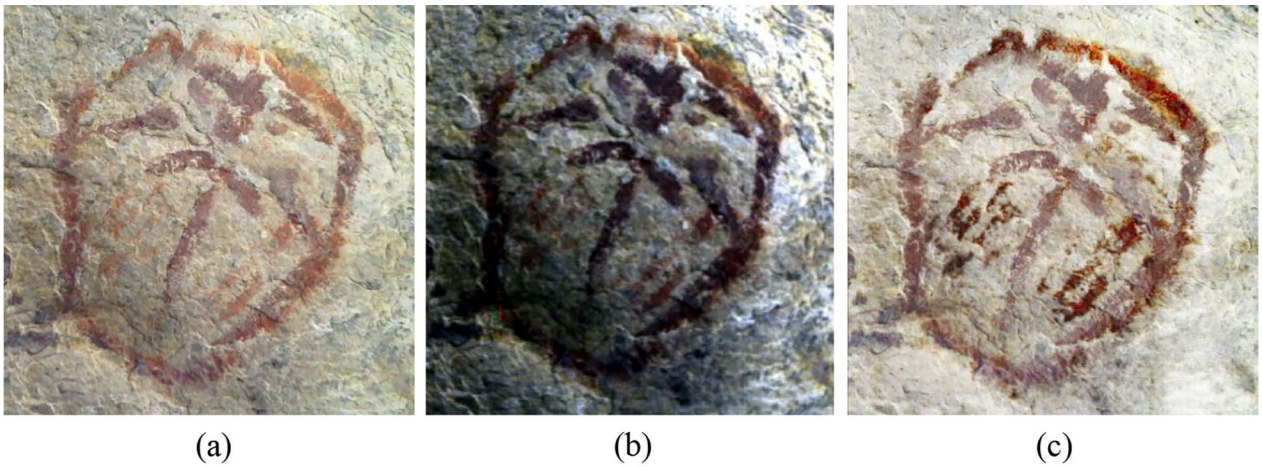

Fig. 9 Superposition result of "facial" information. (**a**) RGB images; (**b**) HSI analog RGB image (R:598.60 nm, G:548.55 nm, B:449.35 nm); (**c**) Overlaying results

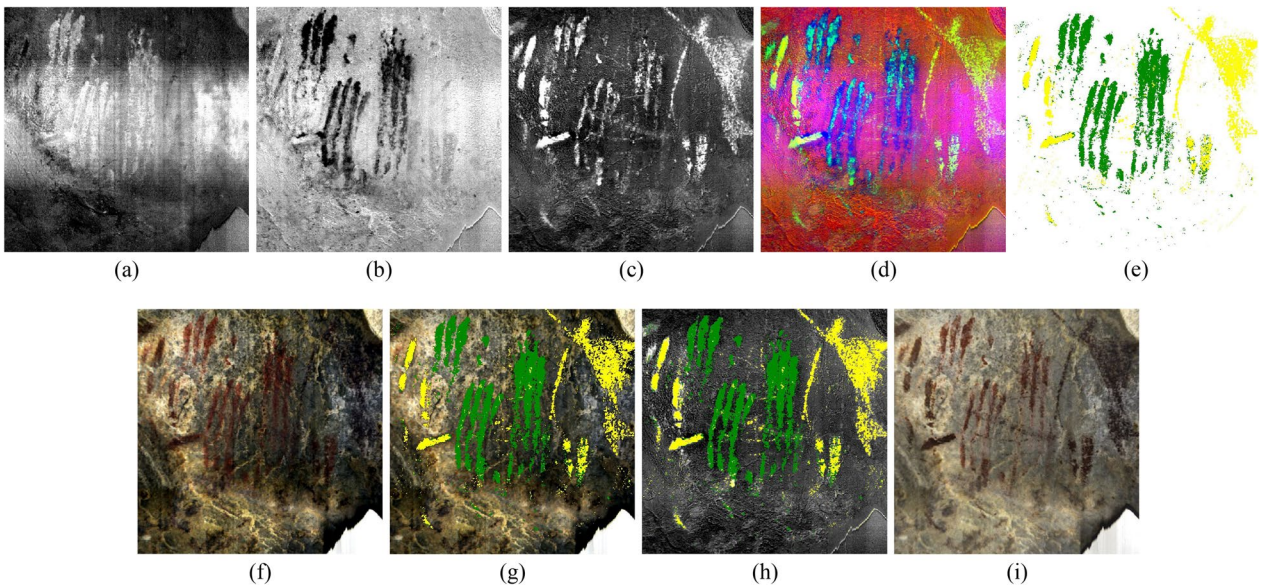

Fig. 10 Analysis results of complex visible scenes. (**a**) ICA component #1; (**b**) ICA component #2; (**c**) ICA component #3; (**d**) ICA false-color images (R:(**b**), G:(**c**), B:(**a**)); (**e**) SAM classification results; (**f**) HSI false-color images (R:598.60nm, G:548.55nm, B:449.35nm); (**g**) (**e**) applied to (**f**); (**h**) (**e**) applied to (**c**); (**i**) Results of information superposition. In (**d**), the imagery is distinctly presented in two colors. To differentiate, the green area is named as "Smear," and the yellow area as "Deer"

bottom of the scene, which is absent in other components. As illustrated in Fig. 14b, c. In Fig. 15a, the right region lacks observable animal shapes under visible light. However, in Fig. 14b, d, the body and head of the "Horse" are extracted, while the pigment of its four legs may have completely vanished due to water erosion and weathering.

To ensure that the extracted "Horse" and "Wild boar" are not formed by other factors such as lichens, rock detachment, or artificial excavation, their ICA components are analyzed first. Since the HSI is composed of four HSIs with a size of 512 × 512, to ensure the rationality of classification, each animal in each region is marked individually, and the "Wild boar" and "Horse" are marked separately. The SAM classification was performed with a maximum angle threshold parameter of 0.4, resulting in the classification shown in Fig. 15. Comparison of the ICA component curves for all classification regions revealed that the classification label

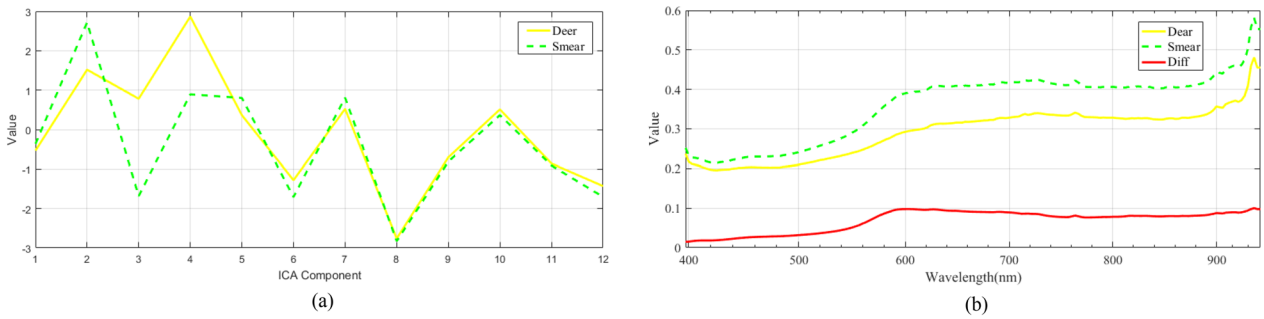

Fig. 11 Information statistics of SAM classification area. (**a**) Component curve of the ICA component; (**b**) The mean spectral curve of the HSI. Where, the "Diff" curve of (**b**) is the value of "Smear" - "Deer"

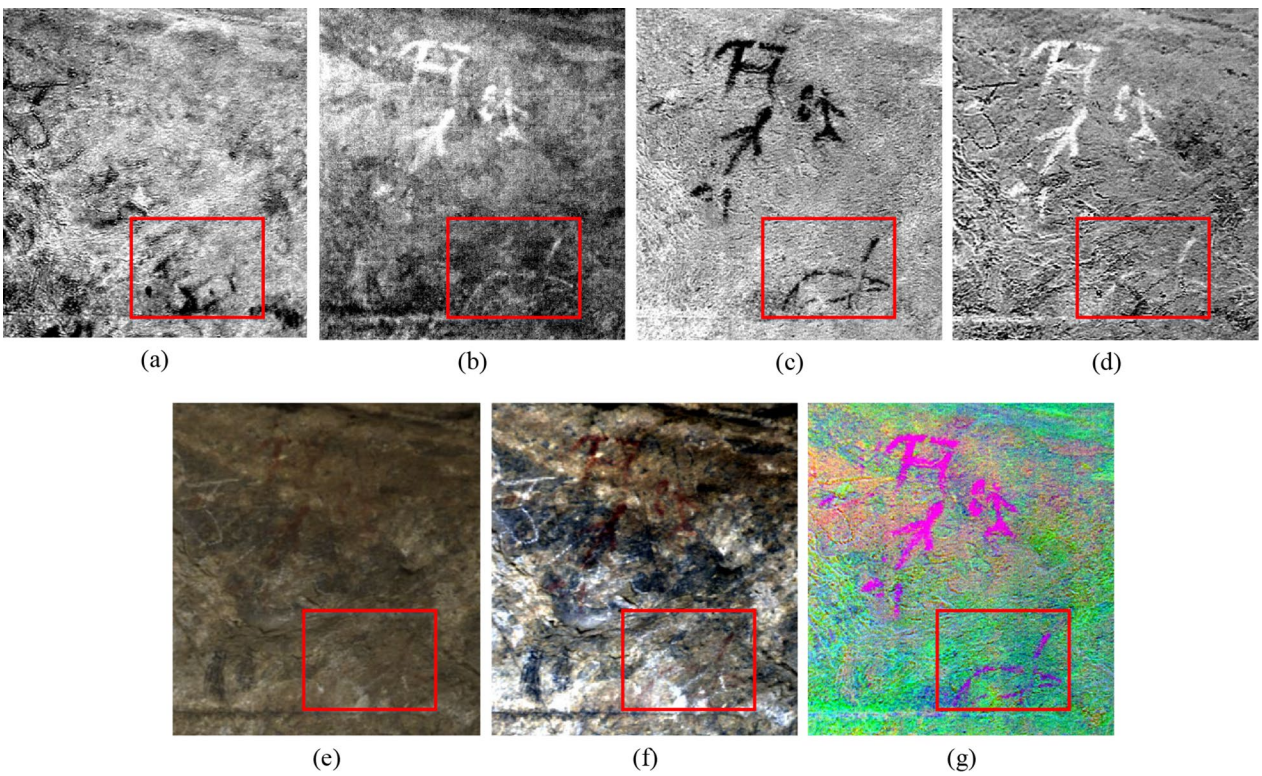

Fig. 12 ICA transformation results of simple invisible scenes. (**a**) Component #1; (**b**) Component #2; (**c**) Component #5; (**d**) Component #7; (**e**) RGB images; (**f**) false-color image synthesized by HSI (R:598.60 nm, G:548.55 nm, B:449.35 nm); (**g**) false-color graphs synthesized by ICA (r: (**b**), g: (**c**), **b**: (**d**))

for "Horse" overlapped significantly with the information from Region 4, so these two categories were merged. Average spectral curves were calculated for the selected regions, and Fig. 15e shows that the characteristic peaks were largely consistent across all regions. The spectral curve for Region 4 differed from other curves between $440nm \sim 680nm$, likely due to uneven illumination during data acquisition. However, after $680nm$, the characteristic peaks for Region 4 aligned with those from other regions, indicating that the extracted depictions of "Wild boar" and "Horse" were painted using the same pigment and during the same period.

Furthermore, on the right side of the Region 4 in Fig. 4, there is an area where red pigment has been applied, as shown in Fig. 16a under visible light (the Region 5 in Fig. 4). Upon conducting ICA transformation on this scene, its information is predominantly represented by thirteen ICA components. The image of "Horse 2"

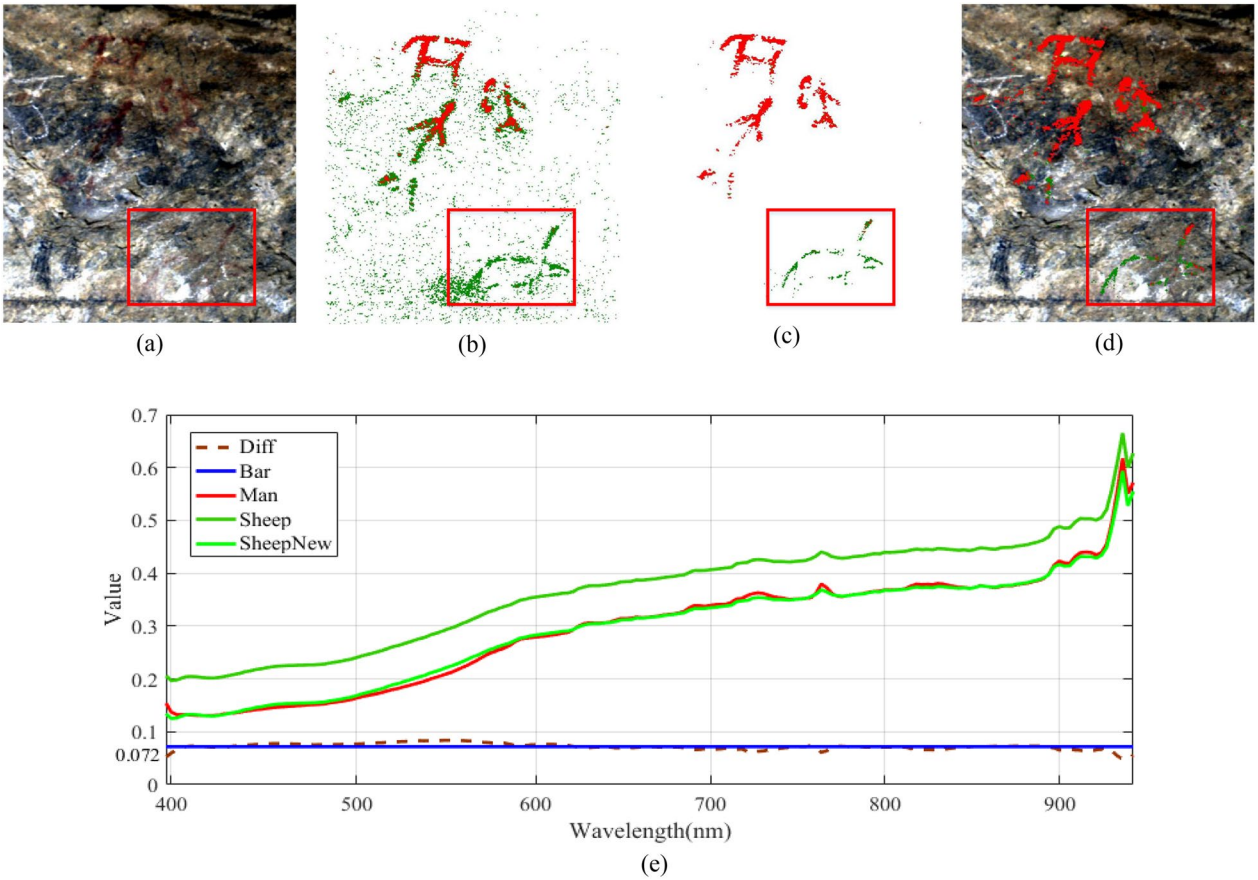

Fig. 13 Region analysis of simple invisible scenes. (**a**) Pseudo-color diagram synthesized by HSI (R:598.60 nm, G:548.55 nm, B:449.35 nm); (**b**) SAM classification results; (**c**) Noise reduction applied to (**b**); (**d**) (**c**) applied to (**a**); (**e**) Regional spectral analysis. The curve "SheepNew" is the result of "Sheep"−"Bar". In (**b**) and (**c**), the imagery is distinctly presented in two colors. To differentiate, the green area is named as "Sheep," and the red area as "Human"

detached from ICA components #3 to #8. In Fig. 16b, c, apart from the "Horse 2", there is an anthropomorphic figure ("Human1") that has been separated, with its "feet" particularly noticeable in Fig. 16c. Additionally, a complex pattern is also isolated in Fig. 16b ("Human2"). To analysis ICA components, both *K*-Means and SAM are utilized with 15 classes. For *K*-Means, the threshold is set to 5 with a maximum of 1000 iterations. In SAM classification, 2–3 classes are chosen for each of the first six components, with a maximum angle parameter of 0.5 radians. After excluding irrelevant areas such as background, rock surfaces, and cracks, only the main classification areas are retained in all results. Among them, *K*-Means retains 3 regions, while SAM retains 5 regions, as shown in Fig. 16d, e. Despite the absence of two "Horse" results in the classification of Fig. 16d, "Human1" and "Human2" patterns can still be identified compared to Fig. 16e. Neither method successfully identified the "feet". Spectral analysis of Fig. 16e reveals that the spectral curves of "Human1" and "Human2" exhibit higher similarities, while the three regions representing "Horse" share closer spectral characteristics. This suggests that Fig. 16e encompasses information pertaining to both "Human1" and "Human2". The lack of clustering classification for the "feet" pattern may be attributed to the limited presence of pigments on the rock surface, resulting in its separate extraction as two distinct components (Fig. 18)

Discussion

The anthropomorphic figure

One of the key findings of this work lies in the discovery of the anthropomorphic figure ("Human1") in Fig. 16e.

The images similar to the Fig. 16d were mainly discovered in the Altai region. Their main features include

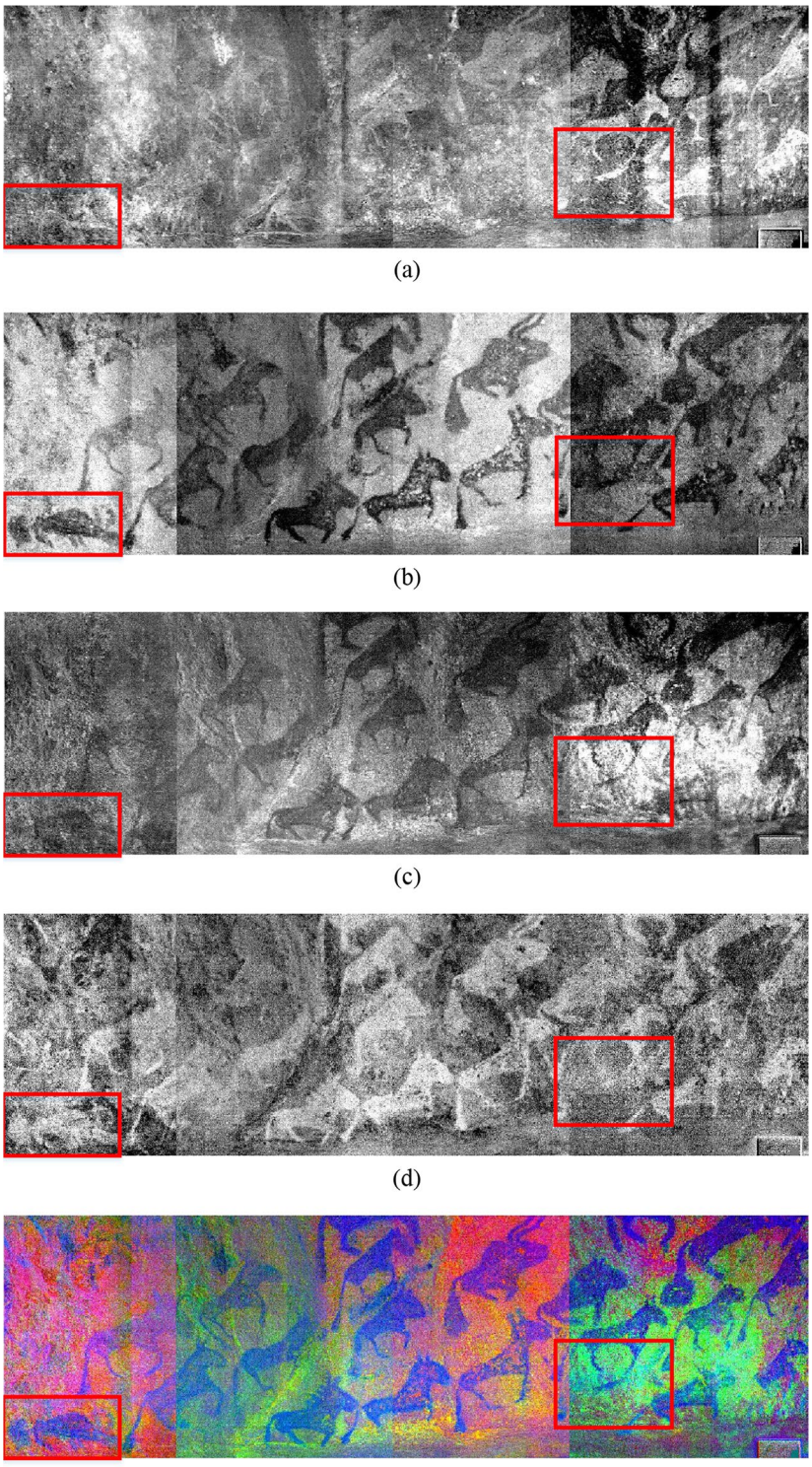

Fig. 14 ICA transformation results of animal group. (**a**) Component #9; (**b**) Component #10; (**c**) Component #11; (**d**) Component #16; (**e**) false-color images synthesized by ICA (r: (**b**), g: (**c**), **b**: (**d**)). The image is a composite of hyperspectral data taken under the same conditions, from left to right in this region 1 to 4

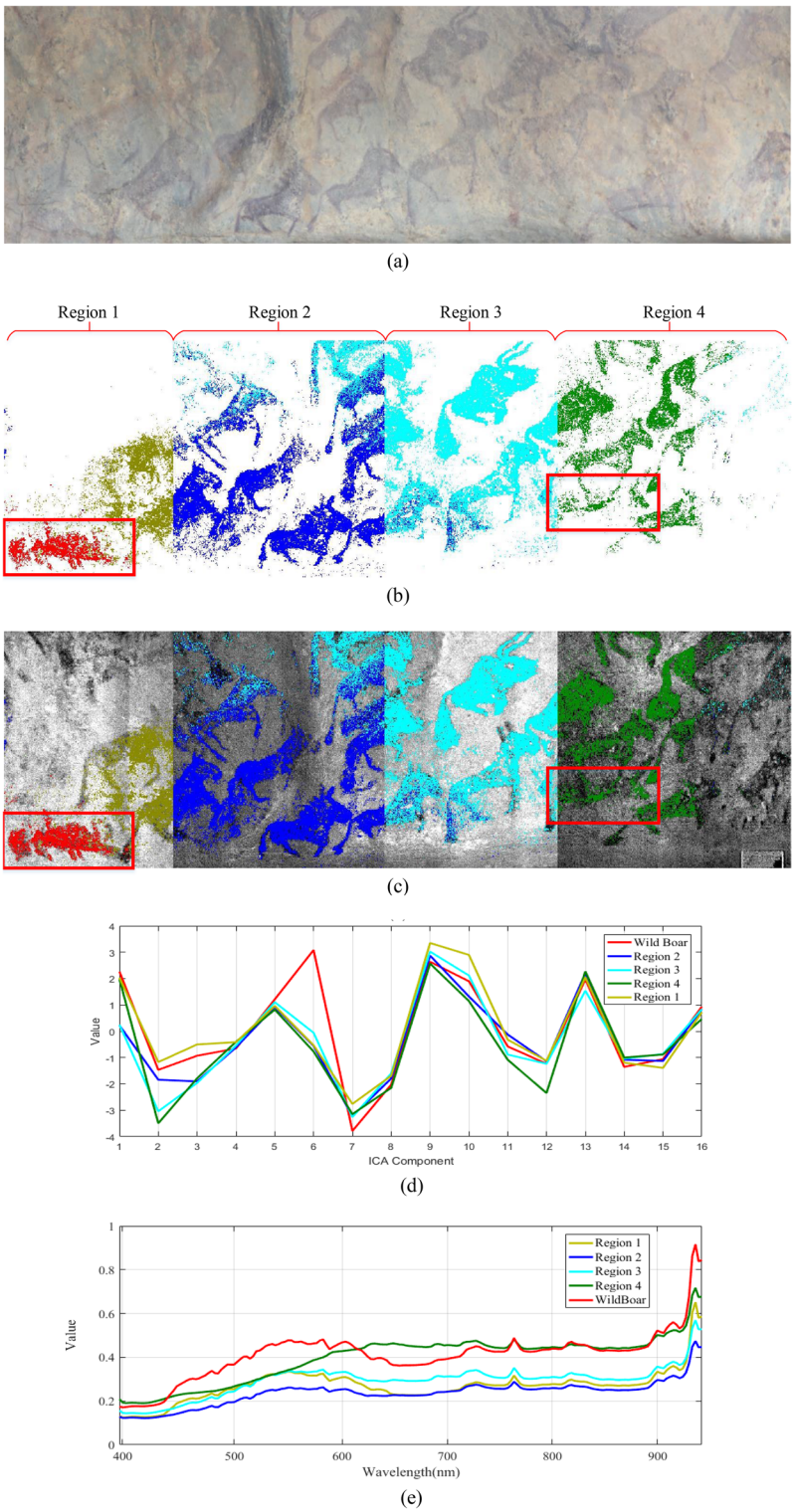

Fig. 15 SAM classification results. (**a**) true colour images; (**b**) SAM classification results; (**c**, **b**) applied to the ICA transform component #10; (**d**) Component curve of ICA component; (**e**) Average spectral curves of hyperspectral images

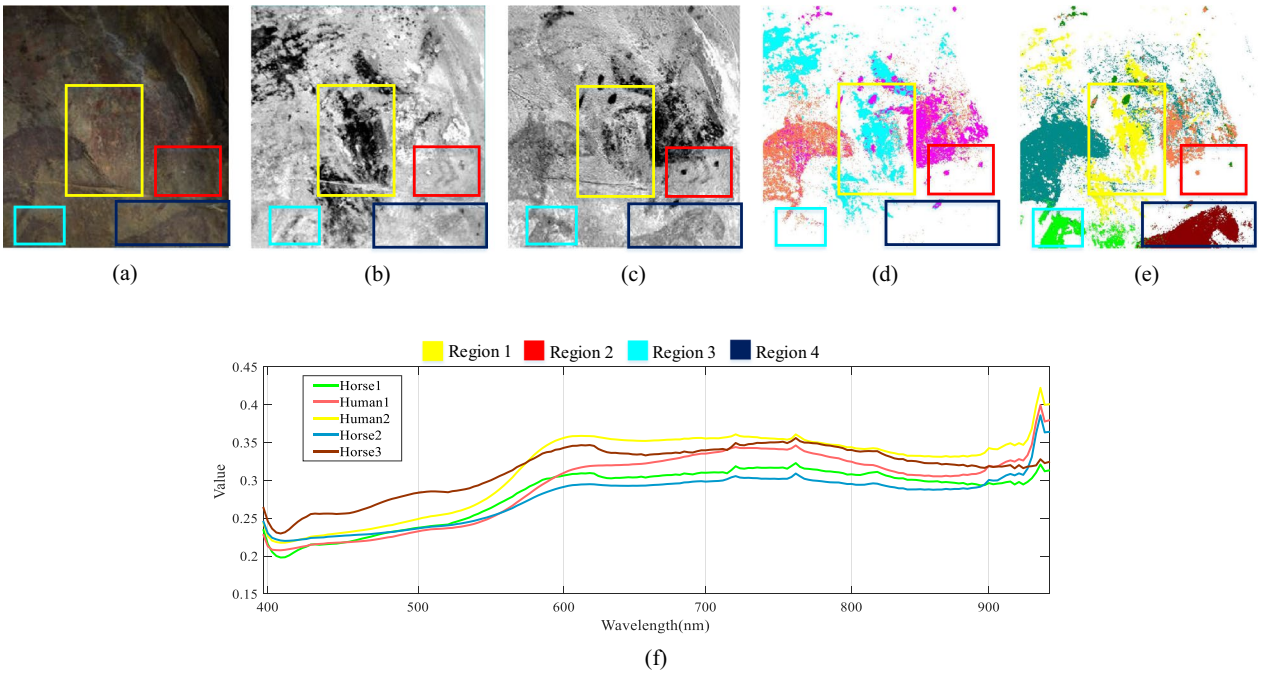

Fig. 16 The result of anthropomorphic figure. (**a**) true colour images; (**b**) ICA transform component #2; (**c**) ICA transform component #5; (**d**) K-Means applied to ICA transformation; (**e**) SAM applied to ICA transformation; (**f**) The average spectral curve of the SAM classification region

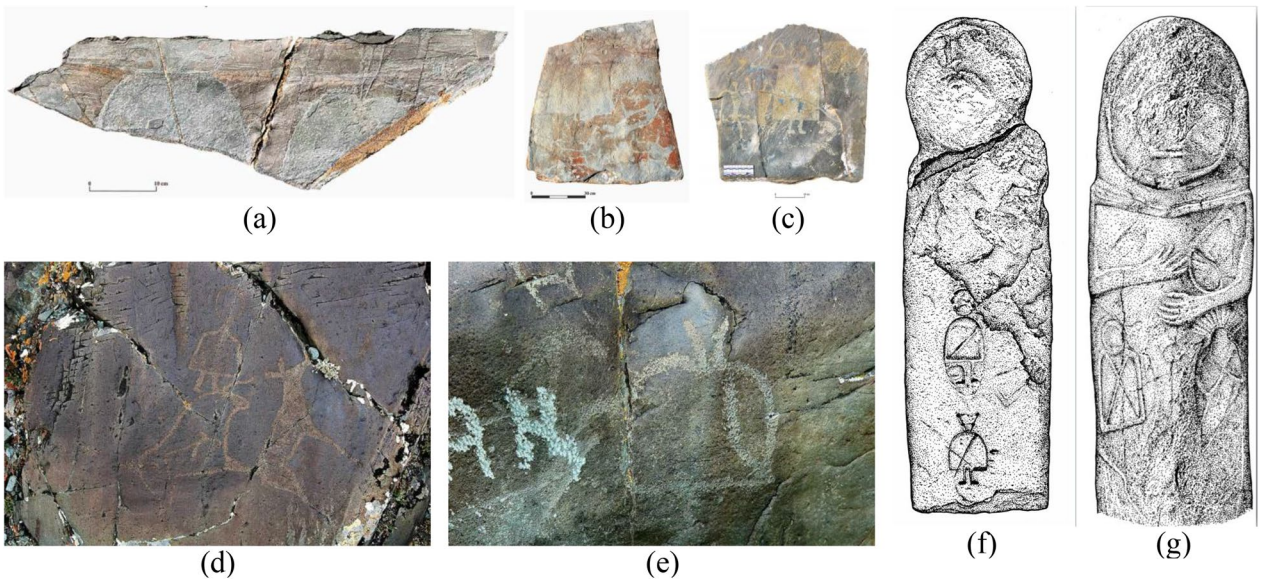

Fig. 17 Similar anthropomorphic patterns found in the Altai Region. (**a**–**c**) Anthropomorphic patterns carved on the surface of a stone slab at the Khar Chuluut1 site [39][Link]. (**d**, **e**) are anthropomorphic patterns in petroglyphs of Tsagaan Salaa and Baga Oigor river basins in northwestern Mongolia[Link]. (**f**, **g**) are anthropomorphic patterns on the surface of the stone figures present in the Burzin Alpablak cemetery (illustration from [40])

a torso in a "bell-shaped" or "cloak-like" form, decorated with "antler-like" ornaments on the head, and legs and feet connected in an "L" shape. Similar patterns are found at the Khar Chuluut-1 site [39] (Fig. 17a–c), and the carbon-14 dating results of the similar ritual constructions at nearby sites indicated that the ritual enclosures belonged to the Chemurcheck cultural were builded no later than the mid-3rd millennium BC. This conclusion

Fig. 18 Two complete deer stones found at Huahaizi No. 3 site in Qinghe County, Altay Region, Xinjiang (illustration from [47])

also had been supported by the AMS dates from other smaller ritual stone constructions [41]. In the Altay Prefecture, similar anthropomorphic pattern also primarily accompanied with the remains belonged to the early period of the Chemurchek culture [42]. Thus, our team posits that the certain images Dunde Bulaq I site were created during the early stage of Chemurchek culture. The new findings provides crucial chronological evidence to estimate the age of Dunde Bulaq complex.

Additionally, in Fig. 16f, the spectral curves of "Human1" and "Horse2" display similar spectral peaks and valleys, indicating their use of closely related pigments. Combined with the study of Gantulga et al. [43] on the image features of Dunde Bulaq I site, our team leans towards considering the animal images and anthropomorphic images in Fig. 4 as both belonging to Chemurchek cultural heritage sites. Based on current findings, anthropomorphic images often encircle animal or other anthropomorphic patterns as central elements in the composition [39]. This phenomenon is also observed in the Dunde Bulaq I site. In Fig. 16c, the toes of the anthropomorphic image seem intentionally directed towards the left side where "Horse3" is depicted. Although existing studies indicate the presence of dairy consumption during the Chemurchek culture [44], Dong et al.'s [45] analysis of carbon and nitrogen isotopes in Bronze to early Iron Age human bones from the Altai region suggests that hunting remained an essential supplementary source of diet during this period. Hunting is a significant theme in rock art of hunter-gatherer societies, both in the Altai region and globally. Hence, we speculate that the anthropomorphic images in the Chemurchek culture are symbolic representations associated with human hunting activities.

The "Blush" in "facial" figure

From field observations, we found that symbols constituted of three slashes, resembling "Blush" (Fig. 6), primarily exist in the Dunde Bulaq I site and exhibit minimal superposition with other patterns in the rock art. This special symbol is often found in the deer stone distributed in the Altai region, Fig. 18. The deer stone was one of the most emblematic monument remains during the Late Bronze Age in Eurasian Steppe and combining with the Khirgisuur constituted a special cultural phenomenon which known as "Deer Stone-Khirgisuur culture [48]." The Altay Prefecture own the most deer stones in China, especially in the Qinghe County bordering on the Mongolia [47]. Among the more than 1,600 deer stones, there are 333 deer stones with 1 to 5 diagonal lines, and more than 70% of deer stones with three diagonal lines [48]. The creators typically use the three grooves to represent "human faces" [49], yet this remains speculative among various interpretations [50, 51]. But until now, the specific meaning of diagonal slashes are not clear.

Painting of deer stones is not an isolated occurrence. Traces of red pigment are still visible within the three grooves of some deer stones [50]. Research by Esin et al. [46] indicates that painting does not always

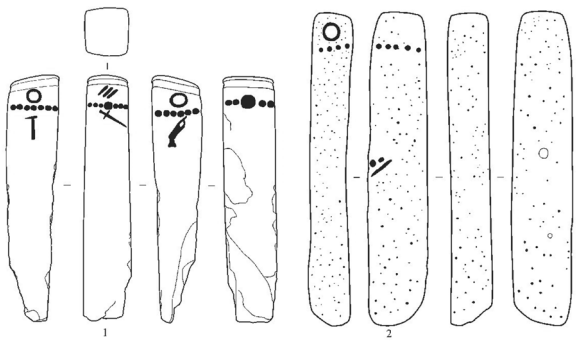

Fig. 19 (**a**) Symbols similar to grooves on the surface of the deer stone found at Nistaforovka (illustration from [46]); (**b**) The short line symbols concentrated on the upper part of the wall of the Dunde Bulaq I rock art site

subordinate to carving skills. Instead, it can independently serve in creating visual images. Simultaneously, typical symbols on deer stones occasionally painted on the rocks. Intriguingly, Dunde Bulaq rock I art site, similar to the Nistafarovka rock art site [46], lies outside the core region of deer stone distribution, as shown in Fig. 19. Based on this observation, we are inclined to consider the "Blush" as special symbols which can be used independently.

In the analyses of the Section "Simple visible scenes", we note that the blue area represented by the "Blush" experiences superimposition by the red area represented by the "Outline." However, this superimposition does not entirely disrupt the integrity of either element; rather, it appears as a conscious reworking of the original imagery. O'Sullivan [52] categorize the "replication behavior" present in rock art into three types: replication of images, replication of places, and replication of actions. The relationship between the "Outline" and the "Blush" seems more akin to the second type of replication behavior, wherein later images incorporate earlier ones without obliterating the earlier graphics. This processing of earlier images not only emphasizes the connection between later contributors and earlier creators but also indirectly suggests the possibility of multiple creation stages for Dunde Bulaq I site.

The animal group figure

Animal is the most common motif in the Dunde Bulaq rock art site. There are different styles among them. More precisely, highly realistic depictions is found in Dunde Bulaq IV and highly simplified ones in Dunde Bulaq II (Fig. 20) respectivly. While The animal figures in the Dunde Bulaq I, such as those in Figs. 14 and 15, fall somewhere between realism and simplification. Based on the general rules of style development, the depictions on Dunde Bulaq IV may have been created during an earlier stage than others.

Additionally, the figures in Dunde Bulaq IV depict hunting activities, although the animal figures are superimposed rather than interacting with each other. Similar composition can be found in the Aral Tolgoi site in Mongolia. Kubarev et al. [53] compared this to the Kalbak-Tash site in the Russian Altai region and suggested that most of the figures in Aral Tolgoi site may date back to the late Neolithic or early Bronze Age. Given the mobility of hunting populations, the research team believes that the figures in the Dunde Bulaq IV should not date any later than the early Bronze Age.

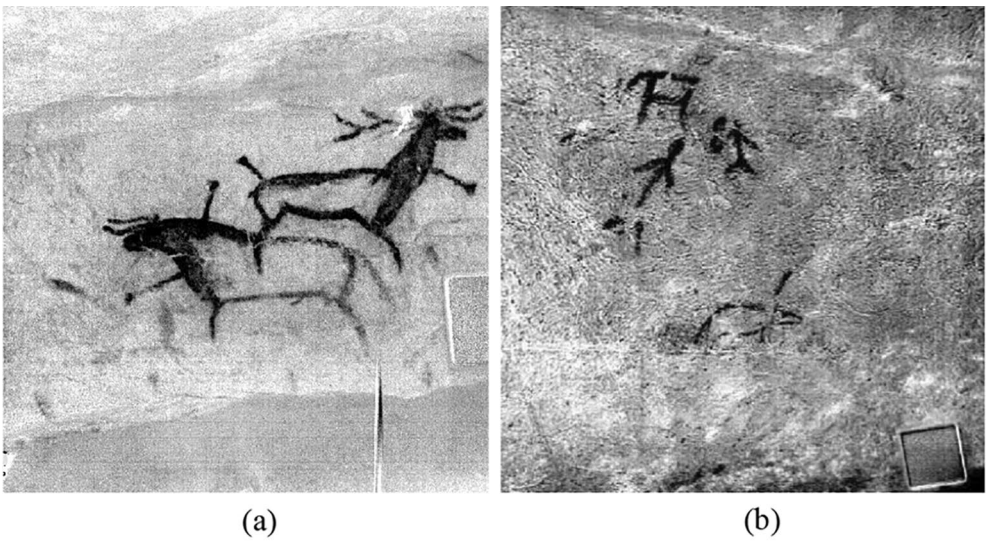

Fig. 20 Animals with different styles. (**a**) the animal in the Dunde Bulaq IV rock art site; (**b**) the animal in the Dunde Bulaq II

In contrast, the animal groups in Dundebulak I predominantly consist of three species: wild horses, wild donkeys, and bison (Fig. 15a). However, in Fig. 15b, the image of the "Wild boar" can be recognized, which has a trunk that gradually narrows from front to back, with its snout being about one-third of its body length and having long fangs. Nevertheless, the image's left side shows a "mushroom-shaped" form, similar to the numerous anthropomorphic figures with mushroom-head and bent legs commonly found in Bronze Age rock art in the Altai region, which are widely regarded as expressions of shamanic beliefs. Therefore, although this image is called "Wild boar" in this work, further research is still needed to determine the meaning behind the depicted figure.

Conclusion

The purpose of this study is to explore the hidden information and determine the age of the Dunde Bulaq rock art site in the Altay Prefecture in the Xinjiang Uyghur Autonomous Region, China, through the collection and analysis of hyperspectral data. Compared to previous research, hyperspectral imaging and analysis tools not only extract image information from the surface of rock art more effectively but also reveal more hidden information on the rocks. This provides comprehensive and accurate evidence for dating the rock art and understanding the imagery. The analysis of the Dunde Bulaq rock art site reveals the existence of multiple creation processes, laying the groundwork for subsequent periodization of the rock art complex. Furthermore, through cross-experiments in classification and clustering of complex images, representative patterns have been separated, showing a high similarity to the cultural element from the early Bronze Age. Moreover, the content depicted in the rock art is closely related to the Chemurchek culture, which supports research on the Chemurchek culture in the region and provides new data for comparative studies of various Bronze Age cultures in the Altai region. The differences in classification within the hyperspectral data indicate that Dunde Bulaq I rock art site may include multiple creation period. Further research on the landscape of this rock art site is necessary to explore its uniqueness.

Acknowledgements
The authors extend special thanks to the School of Heritage Cultural for providing their expertise in support of this work, and to the School of Information & Technology for providing the necessary equipment. Special thanks are extended to the cooperative efforts of the staff at the Altai Regional Museum, whose active collaboration greatly contributed to the success of this study.

Author contributions
Conceptualization: LC, WJ. Methodology: FY, ZX. Formal analysis: CY, ZX, LL. Investigation: CY, LL. Resources: ZB. Data curation: FY, CY. Writing-original draft preparation: FY, CY. Writing-review and editing: LC, WJ. Supervision: LC, WJ, PJ. All authors read and approved the final manuscript.

Funding
Supported by the National Key Research and Development Program of China(No. 2022YFE0203800); by the National Natural Science Foundation of China (No. 62101446); by the International Science and Technology Cooperation Research Plan in Shaanxi Province of China (No. 2022KW-08).

Availability of data and materials
Data sharing is not applicable to this article as no datasets were generated or analysed during the current study.

Declarations

Competing interests
The authors declare that they have no competing interests.

Received: 20 October 2023 Accepted: 12 January 2024
Published online: 02 February 2024

References

1. Garfinkel AP, Austin DR. Reproductive symbolism in great basin rock art: bighorn sheep hunting, fertility and forager ideology. Camb Archaeol J. 2011;21:453–71.
2. Bednarik, R. G. ROCK ART 12 (Academic Press, 2008). https://www.sciencedirect.com/science/article/pii/B9780123739629002739.
3. Jones AM. Rock art and ontology. Ann Rev Anthropol. 2017;46:167–81.
4. Porr M. Rock art as art. Time Mind. 2019;12:153–64.
5. Yu J. Cultural lineage passed down for tens of thousands of years-archaeological excavations at the site of tongtian cave in Jimunai County, Xinjiang. Singapore: Springer Nature Singapore; 2023.
6. Shao H. Discussion on two types of bronze culture in altay region of xinjiang. West Reg Stud. 2008. https://doi.org/10.1636/j.cnki.xyyj.2008.04.011.
7. O'Sullivan R, Shao H. The bronze and iron age rock art of altay prefecture, xinjiang: a synthesis. Rock Art Res J Aust Rock Art Res Assoc (AURA). 2022;39:83–96.
8. Wang B. The polychrome rock paintings in the altay mountains. Silk Road. 2005;3:16–23.
9. Zhang, Z. Shaman rock paintings in the prehistoric period of altay. Collections (2013).
10. Cuparev V, Cevdeendoj D, Yacobson E. Petroglyphs of sulfaraigann-salaa and bagga-oiguide. Novosibirsk: Institute of Archaeology and Ethnography of the Siberian Branch of the Russian Academy of Sciences; 2005.
11. Vanwezer N, Taylor WTT, Bayarsaikhan J, Breitenbach SF, Amano N, Louys J, del Val M, Boivin N, Petraglia M. Hunting, herding, and people in the rock art of mongolia: new discoveries in the gobi-altai mountains. Archaeol Res Asia. 2021;26: 100267.
12. O'Sullivan R. Movement across a 'mountain barrier': Mapping accessibility with rock-art and gis in the altai mountains, eastern eurasia. J Archaeol Sci Rep. 2019;27: 101979.
13. Díaz-Andreu M, Jiménez Pasalodos R, Rozwadowski A, Álvarez Morales L, Miklashevich E, Santos da Rosa N. The soundscapes of the lower chuya river area, russian altai: ethnographic sources, indigenous ontologies and the archaeoacoustics of rock art sites. J Archaeol Method Theory. 2023;30:335–62.
14. Adinolfi G, Carmagnola R, Cataldi M, Marras L, Palleschi V. Recovery of a lost wall painting at the etruscan tomb of the blue demons in tarquinia (viterbo, italy) by multispectral reflectometry and uv fluorescence imaging. Archaeometry. 2019;61:450–8.
15. Shi N, Wang X, Zhang C. The application of infrared thermal wave imaging technology in conservation. J Natl Mus China. 2017;5:149–57.
16. Liggins F, Vichi A, Liu W, Hogg A, Kogou S, Chen J, Liang H. Hyperspectral imaging solutions for the non-invasive detection and automated mapping of copper trihydroxychlorides in ancient bronze. Herit Sci. 2022;10:142. https://doi.org/10.1186/s40494-022-00765-8.
17. Wang J, Sun J, Yu K, Liu C, Wu C, Chen Y, Hu Q. An intelligent identification method of bronze rust category based on grouping lstm and cnn.

J Northwest Univ. 2021;51:778–86. https://doi.org/10.1615/j.cnki.xdxbzr.2021-05-008.
18. Gao Z, Du M, Cao N, Hou M, Wang W, Lyu S. Application of hyperspectral imaging technology to digitally protect murals in the qutan temple. Herit Sci. 2023;11:8. https://doi.org/10.1186/s40494-022-00847-7.
19. Cao N, Lyu S, Hou M, Wang W, Gao Z, Shaker A, Dong Y. Restoration method of sootiness mural images based on dark channel prior and retinex by bilateral filter. Herit Sci. 2021;9:30. https://doi.org/10.1186/s40494-021-00504-5.
20. Schmitt B, Souidi Z, Duquesnoy F, Donzé F-V. From rgb camera to hyperspectral imaging: a breakthrough in neolithic rock painting analysis. Herit Sci. 2023;11:91. https://doi.org/10.1186/s40494-023-00940-5.
21. Defrasne C, Massé M, Giraud M, Schmitt B, Fligiel D, Le Mouélic S, Chalmin E. The contribution of vnir and swir hyperspectral imaging to rock art studies: example of the otello schematic rock art site (saint-rémy-de-provence, bouches-du-rhône, france). Archaeol Anthropol Sci. 2023;15:116.
22. Peng J, Yu K, Wang J, Zhang Q, Wang L, Fan P. Mining painted cultural relic patterns based on principal component images selection and image fusion of hyperspectral images. J Cult Herit. 2019;36:32–9.
23. International Society for Optics and Photonics. A method for the analysis of spectral imaging data from tang tomb murals. Bellingham: SPIE; 2019.
24. Picollo M, Cucci C, Casini A, Stefani L. Hyper-spectral imaging technique in the cultural heritage field: New possible scenarios. Sensors. 2020;20:2843.
25. Castillo E, Bayarri V, Castillo E, Ripoll S. Improved application of hyperspectral analysis to rock art. Appl Sci. 2021;11:1292.
26. Capobianco G, Pronti L, Gorga E, Romani M, Cestelli-Guidi M, Serranti S, Bonifazi G. Methodological approach for the automatic discrimination of pictorial materials using fused hyperspectral imaging data from the visible to mid-infrared range coupled with machine learning methods. Spectrochim Acta Part A Mol Biomol Spectrosc. 2024;304: 123412.
27. Cucci C, Delaney JK, Picollo M. Reflectance hyperspectral imaging for investigation of works of art: old master paintings and illuminated manuscripts. Acc Chem Res. 2016;49:2070–9.
28. Bayarri V, Sebastián MA, Ripoll S. Hyperspectral imaging techniques for the study, conservation and management of rock art. Appl Sci. 2019;9:5011.
29. Skoog B, Helmholz P, Belton D. Multispectral analysis of indigenous rock art using terrestrial laser scanning. Int Arch Photogram Remote Sens Spatial Inform Sci. 2016;41:405–12.
30. Jalandoni A. An overview of remote sensing deliverables for rock art research. Quater Int. 2021;572:131–8.
31. Behmann J, Acebron K, Emin D, Bennertz S, Matsubara S, Thomas S, et al. Specim iq: evaluation of a new, miniaturized handheld hyperspectral camera and its application for plant phenotyping and disease detection. Sensors. 2018. https://doi.org/10.3390/s18020441.
32. Cerrillo-Cuenca E, Sepúlveda M, Guerrero-Bueno Z. Independent component analysis (ica): a statistical approach to the analysis of superimposed rock paintings. J Archaeol Sci. 2021;125: 105269.
33. Shih FY. Image processing and pattern recognition: fundamentals and techniques. Hoboken: John Wiley & Sons; 2010.
34. Beyerer J, Richter M, Nagel M. Pattern recognition: introduction, features, classifiers and principles. Berlin: Walter de Gruyter GmbH & Co KG; 2017.
35. Cerra D, Müller R, Reinartz P. Noise reduction in hyperspectral images through spectral unmixing. IEEE Geosci Remote Sens Lett. 2013;11:109–13.
36. Hyvärinen A, Oja E. Independent component analysis: algorithms and applications. Neural Netw. 2000;13:411–30.
37. Chen Y, Liu X, Lyu S, Wu W, Wang R. Method of hidden strip information extraction from hyperspectral images of ancient paintings. Sens Mater. 2022;34(12):4463–77.
38. Hou M, Cao N, Tan L, Lyu S, Zhou P, Xu C. Extraction of hidden information under sootiness on murals based on hyperspectral image enhancement. Appl Sci. 2019;9:3591.
39. Kovalev A. Megalithic traditions in the early bronze age of the mongolian altai: the chemurchek (Qie'muerqieke) cultural phenomenon // megaliths of the world. Oxford: Archaeopress; 2022.
40. Kovalev AA. Kovalev Ancient statue-menhirs in chemurchek and surrounding territories 2012. Mumbai: SPBGUC; 2019.
41. Wang C-C, Yeh H-Y, Popov AN, Zhang H-Q, Matsumura H, Sirak K, et al. The genomic formation of human populations in East Asia. bioRxiv. 2020. https://doi.org/10.1101/2020.03.25.004606v1.abstract.
42. Jia PWM, Betts AV. A re-analysis of the qiemu'erqieke (shamirshak) cemeteries, Xinjiang, China. J Indo-Eur Stud. 2010;38:275.
43. Gantulga J-O, Turbat T. Rock art studies in Mongolia. Oxford: Archaeopress Publishing Ltd; 2021.
44. Wilkin S, Ventresca Miller A, Taylor WT, Miller BK, Hagan RW, Bleasdale M, et al. Dairy pastoralism sustained eastern eurasian steppe populations for 5000 years. Nat Ecol Evolut. 2020. https://doi.org/10.1038/s41559-020-1120-y.
45. Dong W, An C, Yu J, Chen X. A study on the ecological niche of residents during the bronze and early iron age in Altai region, Xinjiang - based on skeletal isotopes. West Regions Stud. 2022. https://doi.org/10.1636/j.cnki.xyyj.2022.01.005.
46. Esin Y, Magail J, Yeruul-Erdene C, Gantulga J. Paint on deer stones of mongolia. Archaeol Ethnol Anthropol Eurasia. 2017;45:79–89.
47. Institute of Archeology, C., Bureau, A. P. C. R. & Bureau, Q. C. C. R. The excavation of the huahaizi no. 3 site in Ginghe county, Xinjiang. Chin Archaeol. 2017. https://doi.org/10.1515/char-2017-0012.
48. Tsagaan T, Jamiyan-Ombo G, Noost B, Dunburee B, Turbayar N, Erdene-Ochir N-O, et al. Deer stone culture of mongolia and meigh. Ulaanbaatar: Munkhiin useg LLC; 2022.
49. Fitzhugh WW. Mongolian deer stones, European menhirs, and Canadian arctic inuksuit: collective memory and the function of northern monument traditions. J Archaeol Method Theory. 2017;24:149–87.
50. Tishkin AA. Advancing archaeological research of the Mongolian Altai through the scientific study of deer stones: new discoveries from buyant valley. Asian Perspect. 2020;59:453–77.
51. Dimaadjav E. About the new classification of deer stones. News Lab Anc Technol. 2021;17:90–109.
52. O'Sullivan R. Replication in rock art past and present: a case study of bronze and iron age rock art in the Altai, Eastern Eurasia. J Archaeol Method Theory. 2021;28:387–412.
53. Kubarev V. Biluut-tolgoi: a new rock art site in Mongolia. Archaeol Ethnol Anthropol Eurasia. 2007;31:63–8.

Publisher's Note